

Frequency response experiments of eye-vergence visual servoing in lateral motion with 3D evolutionary pose tracking

Hongzhi Tian¹ · Yu Cui¹ · Mamoru Minami¹ · Akira Yanou²

Received: 8 April 2016 / Accepted: 10 August 2016 / Published online: 15 September 2016
© ISAROB 2016

Abstract Visual servoing towards moving target with hand-eye cameras fixed at hand is inevitably affected by hand dynamical oscillations. Therefore, it is difficult to make target position keep always at the center of camera's view, as nonlinear dynamical effects of whole manipulator stand against tracking ability. To overcome this defect of the hand-eye fixed camera system, an eye-vergence system has been put forward, where the cameras could rotate to observe the target object. The visual servoing controllers of hand and eye-vergence are installed independently, so that it can observe the target object at the center of camera images through eye-vergence function. The dynamical superiorities of eye-vergence system are verified through frequency response experiments, comparing with hand tracking performances and the proposed eye-vergence tracking performances. This paper analyzes the performance of 3D-object position and orientation tracking, in which orientation representation method is based on quaternion, and the orientation tracking results are shown with more comprehensive analysis of system performance.

Keywords Visual servoing · Eye-vergence · Model-based matching · Quaternion

1 Introduction

Nowadays, in the field of robot vision, the control method that is called as visual servoing attracts attentions [1–4], can be classified into three major groups: position-based [5], image-based [6, 7], and hybrid visual servoing [8, 9].

The visual servoing, a method for controlling a robot using visual information in the feedback loop, is expected to be able to allow the robot to adapt to changing or unknown environments. Some methods have already been proposed to improve observation abilities, using stereo cameras [10], multiple cameras [11], and two cameras; with one fixed on the end-effector and the other one fixed in the workspace [12]. These methods obtain multiple different views to observe an object by increasing the number of cameras.

Recent researches on visual servoing are limited generally in a swath of tracking an object while keeping a certain constant distance [10, 13, 14]. However, the final objective of visual servoing seems to lie in approaching the end-effector to a target object and then work on it, like grasping. In this case, the desired relation between cameras and the object is time varying, so such eye-vergence camera system is indispensable to keep suitable viewpoint all the time during the approaching visual servoing, utilizing the changeable cameras' eye direction, so as to look at the target in the center of camera images. This advantage of eye-vergence can be called "kinematical merit".

It is easy to catch up to the object by the head's motion of human in the case of the object moving slowly, but when the object become moving faster and faster, human's

This work was presented in part at the 21st International Symposium on Artificial Life and Robotics, Beppu, Oita, January 20–22, 2016.

✉ Hongzhi Tian
psnc8ytd@s.okayama-u.ac.jp

Akira Yanou
yanou-a@mw.kawasaki-m.ac.jp

¹ Division of Mechanical and Systems Engineering, Graduate School of Natural Science and Technology, Okayama University, 1-1-1 Tsushima-naka, Kita-ku, Okayama 700-8530, Japan

² Department of Radiological Technology, Kawasaki College of Allied Health Professions, Kurashiki, Japan

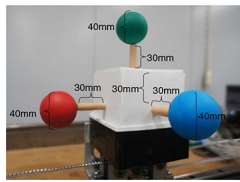


Fig. 1 3D marker

face can hardly keep position squarely to the object, while human’s eye can still keep staring at the object, because of its small mass and inertial moment. This another advantage of eye-vergence can be called “dynamical merit”.

These merits of eye-vergence concerning kinematical and dynamical effects are deemed to be important and useful to keep control stability of closed loop using visual feedback. Therefore, in this report, the merits of eye-vergence visual servoing for tracking that enables the target to be seen at the center of images and avoids the influences of aberration of lens have been experimentally confirmed using eye-vergence function.

In the previous study [15], the system performance of position tracking has been analyzed in detail. However, for three-dimensional objects, except for the position tracking, the orientation tracking is also necessary. In this paper, we obtain the orientation tracking data of the system through the experiments in lateral direction. By conducting pose orientation and position tracking frequency experiment, the stable tracking ability can be confirmed based on the experiment results.

2 3D pose tracking method

In this paper, as shown in Fig. 1, a 3D-ball-object is used as 3D target object, whose size and color are known. However, other target with different kinds of shape can also be measured by model-based matching strategy if its character is given, for example, a model of fish is used to track fish in real time in [10, 16] a model of human face is used for human detection, in which perspective projection is utilized as projection transformation.

2.1 Model-based matching

Dual-camera eye-vergence approach has been described in detail, the following is summarized explanation about real-time pose tracking method [17]. The 3D solid model named S of a rectangular block is shown in Fig. 2 (on the top). The set of coordinates inside of the dotted line block named \mathbb{R} in Fig. 2 means searching space, where pose tracking is conducted on an assumption that the 3D marker in Fig. 1 exists in the space \mathbb{R} .

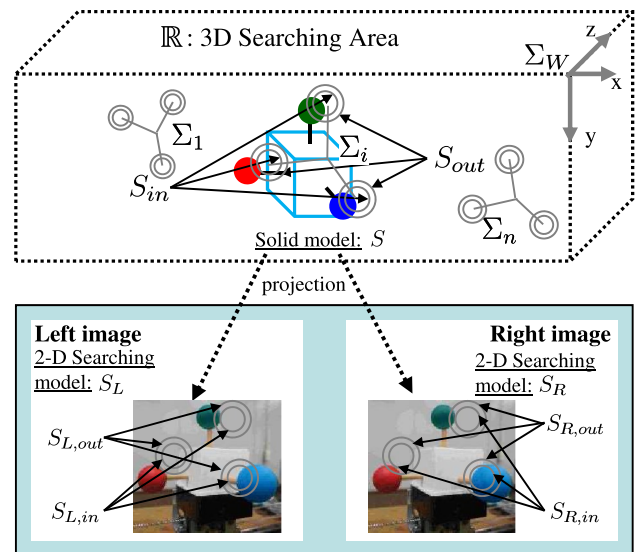


Fig. 2 Definition of a solid model and left/right searching models

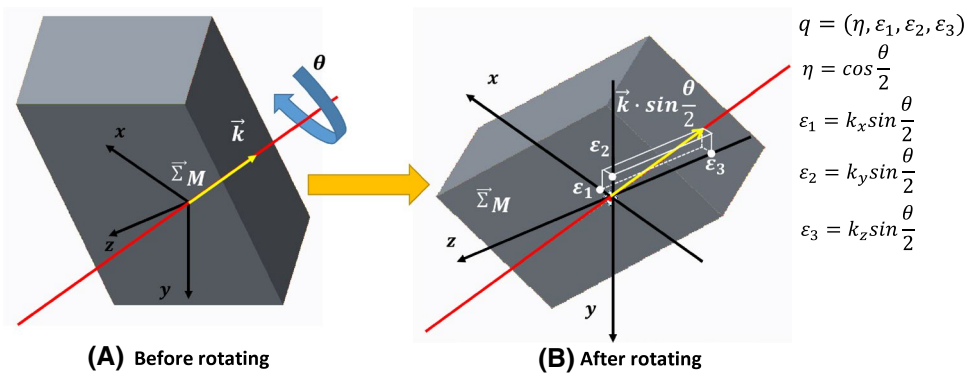
The model to detect 3D-ball-object has the same 3D structure with the 3D-ball-object. The model is represented in \mathbb{R} by three double circles with light color, where inside of inner wide is named as S_{in} , and space between S_{in} and outer circle is named S_{out} .

The i th 3D model is represented by Σ_i , whose pose is assumed to be defined by chromosome

$$\underbrace{10 \dots 10}_{12\text{bit}} \underbrace{11 \dots 01}_{12\text{bit}} \underbrace{01 \dots 10}_{12\text{bit}} \underbrace{\varepsilon_1}_{12\text{bit}} \underbrace{\varepsilon_2}_{12\text{bit}} \underbrace{\varepsilon_3}_{12\text{bit}} = 10 \dots 10 11 \dots 01 01 \dots 10 11 \dots 10 10 \dots 10 10 \dots 01$$

Since the number of chromosome is n , S_{in} and S_{out} are renamed as $S_{in,k}$, $S_{out,k}$ ($k = 1, 2, \dots, n$). Note that the 3D model composed of $S_{in,k}$ and $S_{out,k}$ which are 3D models, the sizes of the balls projected into 2D image of left camera and right one from 3D model are different, since the camera depth distance of each ball is different in 3D space \mathbb{R} in Fig. 2. Projecting S_{in} and S_{out} onto the 2D coordinates of left camera Σ_{iL} and right camera Σ_{iR} , and the left and right 2D searching models, named S_L and S_R , are calculated and shown in Fig. 2 (on the bottom). Color information is used to search for the target object in the images. Supposing, there are distributed solid models in the searching space in Σ_W , each has its own pose. To determine which solid model is most close to the real target, a correlation function used fitness function in genetic algorithm (GA) is defined for evaluation. Everyone of S_{in} have three small circles. And everyone of S_{out} have 3 rings. The relative positions of circles and rings are unchanged. Each pair of circle and ring corresponds with a color, and three pairs of circles and rings are corresponding to red, blue, and green. The higher coincidence degree between a circle and corresponding color ball is, the higher fitness is. Conversely, the higher coincidence degree between a ring and the corresponding

Fig. 3 Definition of quaternion in the proposed system



color ball is, lower fitness will be. When the searching model fits to the target object being imaged in the right and left images, then the fitness function gives maximum value. This optimization problem is solved using the GA method.

2.2 Online pose tracking using “multi-step GA” method

For real-time visual control purpose, GA has been employed in a way denoted as “1-Step GA” evolution [18, 20]. The used cameras’ frame rate is 30 fps. That means every 33 ms cameras output a new image to a computer. In the past, subject to computing speed of the computer, GA explore process per frame can be done only once, so it was called as “1-Step GA”. With advances in computing power of computers, the system can now explore multiple GA explore processes in each frame (actually 9 times). Accuracy has also been improved. Now it is renamed as “Multi-Step GA”.

2.3 Orientation recognition method using quaternion

The methods widely used to represent the orientation of 3D object are Euler angles, angle–axis representation, and rotation quaternion. The first two methods are easy to understand. However, because the orientation singularities exist in the Euler angles and angle–axis representation methods, quaternion representation [19] has been adopted. The definition of unit quaternion is shown in Fig. 3. On the basis of axis–angle representation, a unit vector k indicates direction, and an angle θ describes the magnitude of rotation around the axis. Using k and θ , quaternion $q = \{\eta, \epsilon\}$ is defined as follows:

$$\epsilon = \sin \frac{\theta}{2} k, \tag{1}$$

where

$$\epsilon = [\epsilon_1, \epsilon_2, \epsilon_3]^T, \quad k = [k_x, k_y, k_z]^T. \tag{2}$$

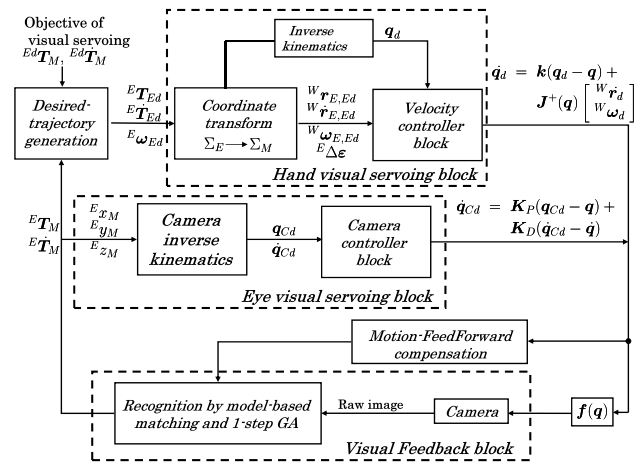


Fig. 4 Block diagram of the hand-visual servoing system

η is the scalar part of the quaternion, and ϵ is the vector part of the quaternion. They satisfy the following relationship of unit quaternion:

$$\eta^2 + \epsilon^T \epsilon = 1. \tag{3}$$

3 Hand and eye-visual servoing controller

3.1 Hand-visual servoing controller

The block diagram of our proposed hand and eye-vergence visual servoing controller is shown in Fig. 4. The hand-visual servoing is the outer loop.

Based on the above analysis of the desired-trajectory generation, the desired hand velocity ${}^W \dot{r}_d$ is calculated as follows:

$${}^W \dot{r}_d = K_{PP} {}^W r_{E,Ed} + K_{VP} {}^W \dot{r}_{E,Ed}, \tag{4}$$

where ${}^W r_{E,Ed}$ and ${}^W \dot{r}_{E,Ed}$ can be calculated from ${}^E T_{Ed}$ and ${}^E \dot{T}_{Ed}$. K_{PP} and K_{VP} are positive definite matrix to determine PD gain.

The desired hand angular velocity ${}^W\omega_d$ is calculated as follows:

$${}^W\omega_d = K_{PO} {}^W R_E^E \Delta \epsilon + K_{VO} {}^W \omega_{E,Ed}, \tag{5}$$

where ${}^E \Delta \epsilon$ is a quaternion error [19] calculated from the pose tracking result, and ${}^W \omega_{E,Ed}$ is computed by transforming the base coordinates of ${}^E T_{Ed}$ and ${}^E \dot{T}_{Ed}$ from Σ_E to Σ_W . In addition, K_{PO} and K_{VO} are suitable feedback matrix gains. The desired hand pose is defined as ${}^W \psi_d^T = [{}^W r_d^T, {}^W \epsilon_d^T]^T$. In addition, the desired joint variable q_{Ed} and \dot{q}_{Ed} is obtained by the following:

$$q_{Ed} = [q_{1d}, \dots, q_{7d}]^T = f^{-1}({}^W \psi_d) \tag{6}$$

$$\dot{q}_{Ed} = J_E^+(q) \begin{bmatrix} {}^W \dot{r}_d \\ {}^W \omega_d \end{bmatrix} \tag{7}$$

where $f^{-1}({}^W \psi_d)$ is the inverse kinematic function and $J_E^+(q)$ is the pseudo-inverse matrix of $J_E(q)$, which is the Jacobian about joint angles q , and $J_E^+(q) = J_E^T (J_E J_E^T)^{-1}$. The manipulator is 7 links, and the end-effector has 6-DoF, so q_1 is set as 0 to remove the redundancy of the robot-PA 10. Using the inverse kinematics, it can make the joint of angles approximately as the desired joint angles. The formula of the desired joint angles was defined in the new controller as

$$\dot{q}_{Ed} = K_P (q_{Ed} - q_E) + J_E^+(q) \begin{bmatrix} {}^W \dot{r}_d \\ {}^W \omega_d \end{bmatrix} \tag{8}$$

where K_P is positive gain.

The hardware control system of the velocity-based servo system of PA10 is expressed as

$$\tau = K_{SP} (q_d - q) + K_{SD} (\dot{q}_d - \dot{q}) \tag{9}$$

where K_{SP} and K_{SD} are symmetric positive definite matrices to determine PD gain.

3.2 Eye-vergence visual servoing controller

The eye-vergence visual servoing is conducted by the inner loop of the visual servoing system, as shown in Fig. 4. In this paper, two pan-tilt cameras are used for eye-vergence visual servoing. Here, the positions of cameras are supposed to be fixed on the end-effector.

For camera system, q_8 is tilt angle, q_9 and q_{10} are pan angles, and q_8 is common for both cameras.

As it is shown in Fig. 5a and b, ${}^E x_{\widehat{M}}$, ${}^E y_{\widehat{M}}$, and ${}^E z_{\widehat{M}}$ express position of the detected object in the end-effector coordinate. The desired angle of camera joints are calculated by:

$$q_{8d} = atan2({}^E y_{\widehat{M}}, {}^E z_{\widehat{M}}) \tag{10}$$

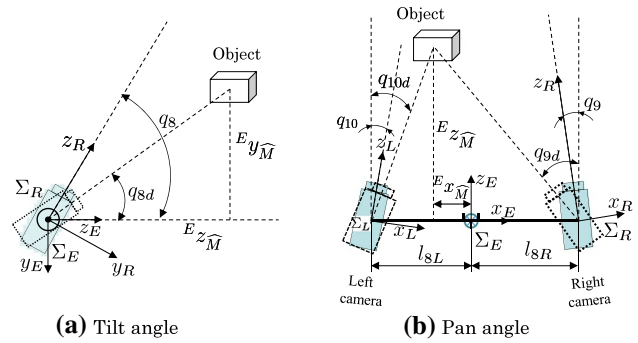
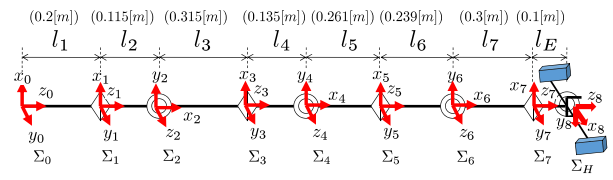
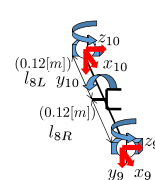


Fig. 5 Calculation of tilt and pan angles



(a) Sketch map of the eye-vergence system



(b) Sketch map of the cameras



(c) Physical map of the cameras

Fig. 6 Frame structure of manipulator

$$q_{9d} = atan2(-l_{8R} + {}^E x_{\widehat{M}}, {}^E z_{\widehat{M}}) \tag{11}$$

$$q_{10d} = atan2(l_{8L} + {}^E x_{\widehat{M}}, {}^E z_{\widehat{M}}) \tag{12}$$

where $l_{8L} = l_{8R} = 120$ [mm] is the camera location. The controller of eye-visual servoing is given by

$$\dot{q}_{8Cd} = K_P (q_{8d} - q_8) + K_D (\dot{q}_{8d} - \dot{q}_8) \tag{13}$$

$$\dot{q}_{9Cd} = K_P (q_{9d} - q_9) + K_D (\dot{q}_{9d} - \dot{q}_9) \tag{14}$$

$$\dot{q}_{10Cd} = K_P (q_{10d} - q_{10}) + K_D (\dot{q}_{10d} - \dot{q}_{10}) \tag{15}$$

where K_P and K_D are positive control gain.

Because the motion of camera motor is an open loop, it is controlled to rotate a certain degree without getting the actual angle during the rotation, which makes the accurate camera angle cannot be got. Therefore, the desired camera angles are input in every 33 ms limited to a certain value.

4 Experiment of hand and eye-vergence visual servoing

4.1 Experimental system

Experiments were taken to verify the effectiveness of the hand and eye-visual servoing system through real robot-PA-10 robot arm-manufactured by Mitsubishi Heavy Industries. In addition, two rotational cameras mounted on the end-effector are FCB-1X11A manufactured by Sony Industries. The frame frequency of stereo cameras is set as 30 fps. The image processing board, CT-3001, receiving the image from the CCD camera is connected to the host computer (CPU: Intel Core i7-3770 , 3.40 GHz).

The structure of the manipulator and the cameras is shown in Fig. 6. The coordinates of the target object and the manipulator in experiment are shown in Fig. 7.

First, an experiment was made in which true object's $x, y, z, \varepsilon_1, \varepsilon_2,$ and ε_3 are assumed to be given to servoing controller. Then, it was carried out the 3 groups of experiments of frequency response. In these experiments, x -position, 3-Dof position, and 6-Dof position/orientation are recognized, respectively. For every group angular velocities of the object, $\omega = 0.314, 0.628,$ and 1.256 [rad/s] are set separately.

4.2 Experiment condition

EO, MO, and EC represent the initial hand pose, initial object pose, and midpoint of round-trip tracking movements of hand, respectively. Therefore, their coordinate systems are defined as $\Sigma_{EO}, \Sigma_{EC},$ and Σ_{MO} separately, as shown in Figs. 7 and 8. The homogeneous transformation matrix from Σ_W to Σ_{EC} and Σ_{MO} is:

$${}^wT_{EC} = \begin{bmatrix} 0 & 0 & -1 & -690 \text{ [mm]} \\ 1 & 0 & 0 & 0 \text{ [mm]} \\ 0 & -1 & 0 & 485 \text{ [mm]} \\ 0 & 0 & 0 & 1 \end{bmatrix} \quad (16)$$

$${}^wT_{MO} = \begin{bmatrix} 0 & 0 & -1 & -1235 \text{ [mm]} \\ 1 & 0 & 0 & -150 \text{ [mm]} \\ 0 & -1 & 0 & 585 \text{ [mm]} \\ 0 & 0 & 0 & 1 \end{bmatrix}. \quad (17)$$

Target object motion function is

$${}^{Ed}\psi_M = [0, -100 \text{ [mm]}, 545 \text{ [mm]}, 0, 0, 0]. \quad (18)$$

Target position and orientation relationship between the object and the end-effector is set as follows:

$${}^{Ed}\psi_M = [0, -100 \text{ [mm]}, 545 \text{ [mm]}, 0, 0, 0]. \quad (19)$$

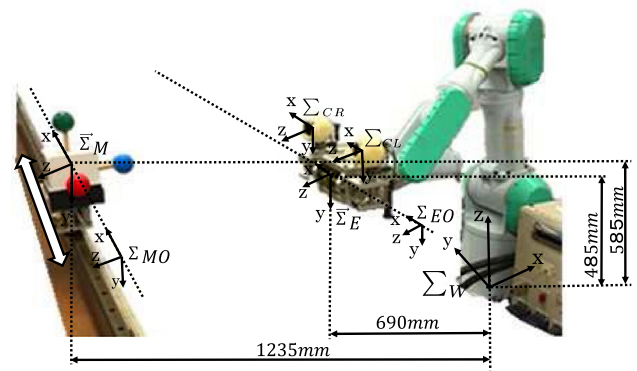


Fig. 7 Object and the visual servoing system

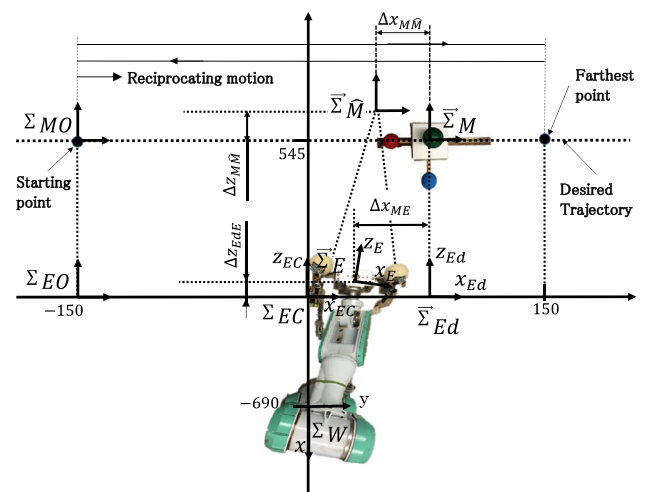


Fig. 8 Object is reciprocating on the trajectory in lateral direction. Object and the system are shown from the $x-z$ plane of Σ_{EC} of hand. The initial position of the object Σ_{MO} , actual object Σ_M , detected object $\Sigma_{\hat{M}}$, initial position of the hand Σ_E , actual end-effector Σ_{Ed} , and theoretical end-effector Σ_{Ed} . At this moment, orientation $\varepsilon \neq 0$, since orientation of Σ_E and the one of Σ_M is different

The object is subjected to reciprocating motion of the sine wave in orbit. Pose relationship of the coordinate system of the object and the visual servoing system are shown in Fig. 7.

4.3 Symbol meaning

M represents the object and \hat{M} represents the estimated object. Then, $\vec{\Sigma}_M$ denotes the coordinate system that moves along with the object. The relationship between coordinate systems, such as the actual pose of the hand $\vec{\Sigma}_E$ or the recognized pose of the object $\vec{\Sigma}_{\hat{M}}$, is shown in Fig. 8. In the figure, $\vec{\Sigma}$ represents a coordinate system moving in the world coordinate system Σ_W . The coordinate system represented

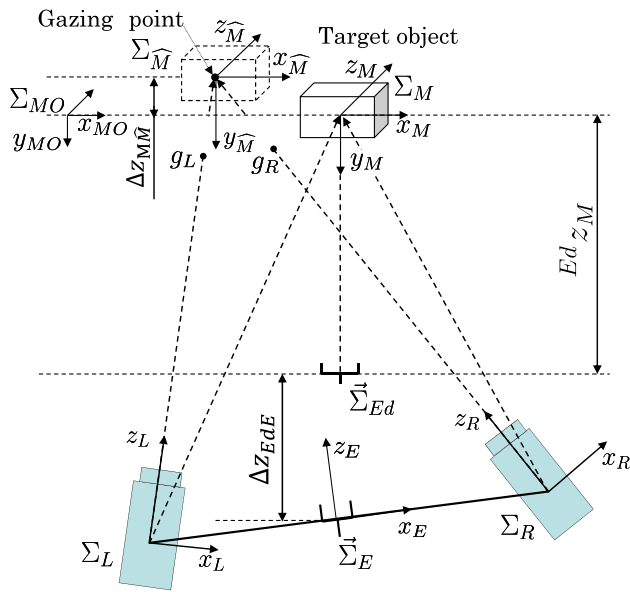


Fig. 9 Cameras' gazing point

by Σ keeps fixed in Σ_W . In other words, $\vec{\Sigma}_E, \vec{\Sigma}_{Ed}, \vec{\Sigma}_M,$ and $\vec{\Sigma}_{\hat{M}}$ are all moving in Σ_W . On the other hand, $\Sigma_{EO}, \Sigma_{EC},$ and Σ_{MO} keep fixed in the world coordinate system Σ_W .

The motion of object M , hand E , and gazing point \hat{M} in the x -axis of Σ_{EC} is represented by ${}^{EC}x_M, {}^{EC}x_E,$ and ${}^{EC}x_{\hat{M}},$ respectively, as shown in Fig. 11. The distance between object and end-effector (hand) is expressed as

$$\Delta i_{ME} = {}^{EC}i_M - {}^{EC}i_E, (i = x, y, z). \tag{20}$$

Tracking error of gazing point:

$$\Delta i_{M\hat{M}} = {}^{EC}i_M - {}^{EC}i_{\hat{M}}, (i = x, y, z). \tag{21}$$

Tracking error of end-effector (hand):

$$\Delta i_{EdE} = {}^{EC}i_{Ed} - {}^{EC}i_E, (i = x, y, z). \tag{22}$$

As shown in Fig. 8 and Eq. (19), the desired value between object and hand is $\Delta x_{ME} = 0, \Delta y_{ME} = -100$ mm, $\Delta z_{ME} = 545$ mm. And, of course, the desired tracking error between gazing point and hand is 0, i.e., $i_{M\hat{M}} = 0$ and $i_{EdE} = 0$.

In the previous research [21], the gazing point was not defined as the left and right eye-sight line intersection but as the intersection g_L of sight line of left camera and the $x_{MO} - y_{MO}$ plane in Σ_{MO} in Fig. 9, so was right camera. Therefore, there were two gazing points $g_L, g_R,$ as shown in Fig. 9. This definition is very different from human eyes. As shown in Fig. 9, to mimic human-eye system, the intersection of both cameras' gazing directions is defined as the

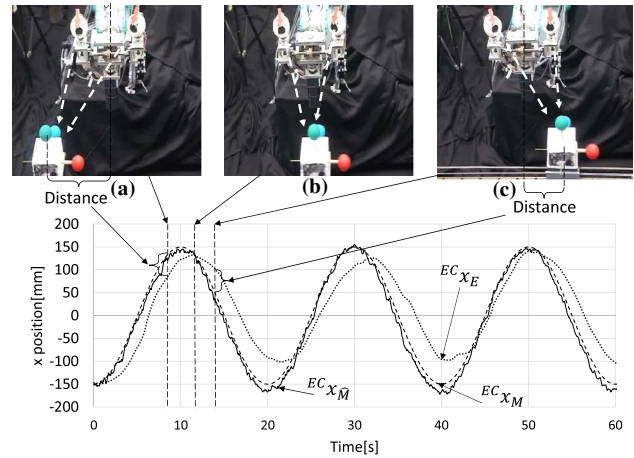


Fig. 10 Eye-vergence system and object position

gazing point of cameras to examine trackability of the eye-vergence system. As the gazing point has been calculated based on the recognition result of the object using multi-step GA, recognition error is included in the estimated gazing point.

4.4 Experiment results

4.4.1 Relation between position diagram and real machine

Figure 10 shows the positional relationship between the hand and the object on the condition that the position and orientation all six variables need to be recognized. In addition, the motion period of the object is $T = 20$ [s]. Movement trajectory of the object M , hand E , and gazing point \hat{M} is represented by dashed line ${}^{EC}x_M,$ dotted line ${}^{EC}x_E,$ and solid line ${}^{EC}x_{\hat{M}},$ respectively. In the case of Fig. 10b, the hand is just in front of the object. In the case of (a) and (c), since the moving velocity of the object is fast, hand is not able to track the object. Since the tracking state of hand is the same as that of hand or camera in fixed camera system, ${}^{EC}x_E$ in the figure also represents the movement of hand or camera in fixed camera system. At this time, it is clear that the distance between the hand ${}^{EC}x_E$ and the object ${}^{EC}x_M$ on the x -axis direction is farther than that between the gazing point ${}^{EC}x_{\hat{M}}$ and target object ${}^{EC}x_M$ of the camera. From the error between ${}^{EC}x_{\hat{M}}$ and ${}^{EC}x_M,$ it can be seen that it is easier for eye-vergence system to track the object than the fixed camera system.

4.4.2 Position tracking result and analysis of the tracking experiment

As the object is reciprocating in the x direction, only the tracking result at the x -axis is given and analyzed, as shown

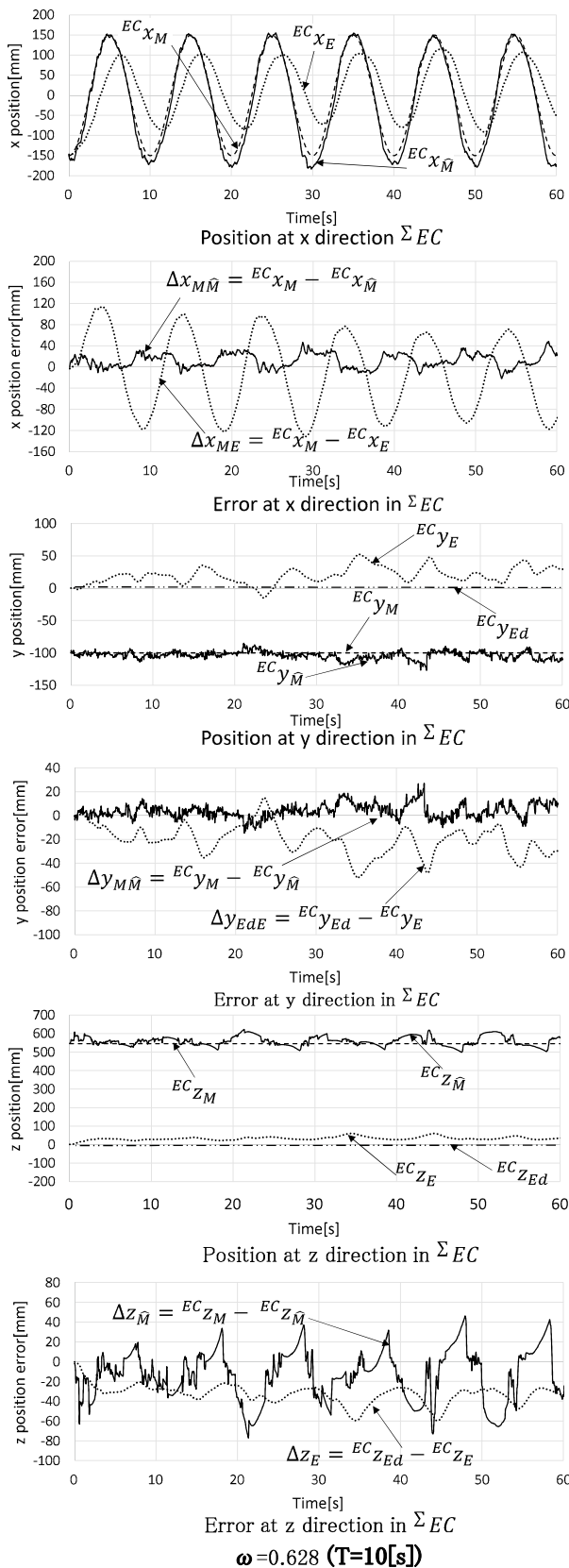


Fig. 11 Movements of actual object M_x , detected object \hat{M}_x , and end-effector E_x in the x , y , and z axes of the center coordinate system of hand Σ_{EC} . The object's pose x , y , z , ε_1 , ε_2 , and ε_3 are recognized by camera

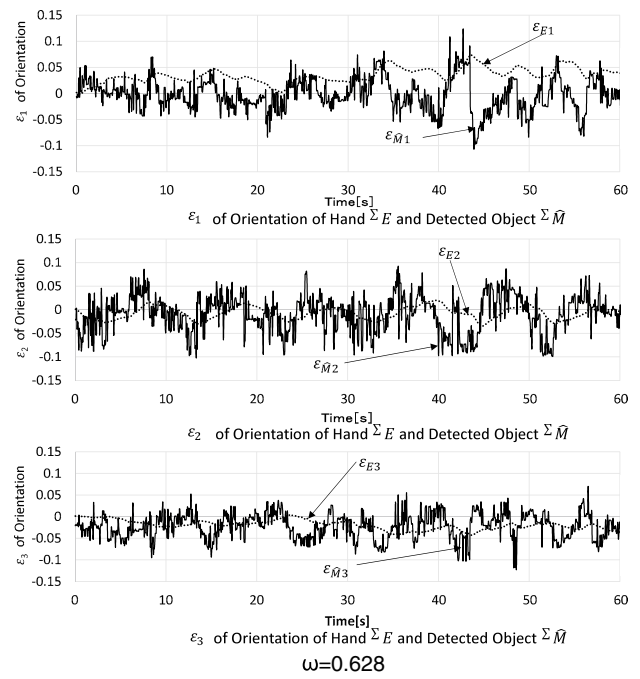


Fig. 12 Quaternion changes of orientation of hand and detected object during tracking movement

in Fig. 11. Simultaneously the movement cycle is 10 s ($\omega = 0.628$). As shown in Fig. 11, it is clear that the motion of hand has delayed against that of the object when the cycle is 10 s. In addition, the deviation of the gazing point is less than that of hand. Therefore, it is obvious that the trackability of the eye-vergence system is better than that of the end-effector.

4.4.3 Orientation tracking result and analysis of the tracking experiment

Orientation tracking result of the detected object and hand is shown in Fig. 12. The same as the tracking status of x , y , and z the quaternion variation of detected object is more frequent than that of hand. Since the camera mass is smaller than manipulator, so the moment of inertia is also smaller than that of manipulator. Therefore, it can adjust faster than manipulator. In Fig. 12, the phases of the detected object ε_{E1} , ε_{E2} , and ε_{E3} are all earlier than that of the hand. That result is consistent with the control procedure. Compared with the end-effector, giving the camera freedom can make the camera more quickly to track the object during its transform of the orientation.

5 Conclusion

In this paper, the eye-vergence visual servoing controller of eye-vergence system has been described in detail. In

addition, the recognition and control results of both orientation and position have been analyzed for the first time by tracking experiment to the 3D marker with 6 degree of freedoms. Finally, it is confirmed that not only position but also orientation trackability of the gazing point of eye-vergence system are better than the trackabilities of the end-effector (hand).

References

- Hutchinson S, Hager GD, Corke PI (1996) A tutorial on visual servo control. *Robot Autom IEEE Trans* 12(5):651–670
- Oh PY, Allen PK (2001) Visual servoing by partitioning degrees of freedom. *Robot Autom IEEE Trans* 17(1):1–17
- Malis E, Chaumette F, Boudet S (1999) 2-1/2-D visual servoing. *Robot Autom IEEE Trans* 15(2):238–250
- Allen PK et al (1993) Automated tracking and grasping of a moving object with a robotic hand-eye system. *Robot Autom IEEE Trans* 9(2):152–165
- Sepp W, Fuchs S, Hirzinger G (2006) Hierarchical featureless tracking for position-based 6-dof visual servoing. In: *Intelligent robots and systems, 2006 IEEE/RSJ international conference*. IEEE
- Hiramatsu T et al (2009) Image-based path following control of mobile robots with central catadioptric cameras. In: *Robotics and automation, 2009. ICRA'09. IEEE international conference*. IEEE
- Tahri O et al (2009) Generic decoupled image-based visual servoing for cameras obeying the unified projection model. In: *Robotics and automation, 2009. ICRA'09. IEEE international conference*. IEEE
- Farahmand AM et al (2009) Model-based and model-free reinforcement learning for visual servoing. In: *Robotics and automation, 2009. ICRA'09. IEEE international conference*. IEEE
- Kim D-J, Lovelett R, Behal A (2009) Eye-in-hand stereo visual servoing of an assistive robot arm in unstructured environments. In: *Robotics and automation, 2009. ICRA'09. IEEE international conference*. IEEE
- Song W, Minami M, Mae Y, Aoyagi S (2007) On-line evolutionary head pose measurement by feedforward stereo model matching. In: *Robotics and automation, 2007 IEEE international conference*. IEEE, pp 4394–4400
- Stavnitzky J, Capson D (2000) Multiple camera model-based 3-D visual servo. *Robot Autom IEEE Trans* 16(6):732–739
- Dune C, Marchand E, Leroux C (2007) One click focus with eye-in-hand/eye-to-hand cooperation. In: *Robotics and automation, 2007 IEEE international conference*. IEEE, pp 2471–2476
- Tahri O, Chaumette F (2005) Point-based and region-based image moments for visual servoing of planar objects. *Robot IEEE Trans* 21(6):1116–1127
- Hamel T, Mahony R (2002) Visual servoing of an under-actuated dynamic rigid-body system: an image-based approach. *Robot Autom IEEE Trans* 18(2):187–198
- Cui Y et al (2015) Analyses about trackability of hand-eye-vergence visual servoing in lateral direction. In: *Applied mechanics and materials, vol 772*. Trans Tech Publications, Switzerland, pp 512–517
- Minami M et al (2001) Visual servoing to fish and catching using global/local GA search. In: *Advanced intelligent mechatronics, 2001. Proceedings. 2001 IEEE/ASME International Conference, vol 1*. IEEE
- Yu F et al (2012) On-line head pose estimation with binocular hand-eye robot based on evolutionary model-based matching. *J Comput Inf Technol* 2(1):43–54
- Suzuki H, Minami M (2005) Visual servoing to catch fish using global/local GA search. *Mechatronics IEEE/ASME Trans* 10(3):352–357
- Song W, Minami M, Aoyagi S (2008) On-line stable evolutionary recognition based on unit quaternion representation by motion-feedforward compensation. *Int J Intell Comput Med Sci Image Process* 2(2):127–139
- Minami M, Song W (2009) Hand-eye motion-invariant pose estimation with online 1-step GA-3D pose tracking accuracy evaluation in dynamic hand-eye oscillation. *J Robot Mechatron* 21(6):709
- Maeda K et al (2012) Frequency response experiments of 3-d pose full-tracking visual servoing with eye-vergence hand-eye robot system. In: *SICE annual conference (SICE), 2012 Proceedings*. IEEE